№ 318/612 – BIV – 15/06/18 – Число полос: 4

Quantum Electronics **48** (6) 573–576 (2018)

https://doi.org/10.1070/QEL00000

Selection of a two-dimensional image edge using polarisation-independent acousto-optic diffraction

V.M. Kotov, S.V. Averin, E.V. Kotov

Abstract. **A method for filtering two-dimensional distributions of light-wave spatial frequencies, based on the use of polarisation-independent acousto-optic (AO) Bragg diffraction, is proposed. This method provides a maximally possible transmission bandwidth of spatial frequencies and a minimum size of the resolved AO element. A selection of a two-dimensional edge in the zero Bragg order is demonstrated. The main theoretical conclusions are experimentally confirmed using a paratellurite AO filter.**

Keywords: *acousto-optic diffraction, Bragg regime, intrinsic optical crystal modes, selection of optical image edge.*

1. Introduction

Acousto-optic (AO) diffraction is one of the efficient methods that are used to select a two-dimensional edge of an optical image during its Fourier processing (see, e. g., [1–4]). In this case, AO elements play a role of spatial-frequency filters. The properties of these filters were investigated in detail in [5, 6]. It was shown that the most important filter characteristics are the spatial-frequency transmission bandwidth, $\Delta f_p = \Delta\Theta_p/\lambda$, and the minimum resolved size of AO element, $d_{min} = 1/\Delta f_p$. These parameters are determined at a level of 3 dB in the case of low efficiency diffraction as [5, 6]

$$\Delta\Theta_p = 0.89V/Lf, \quad d_{min} = 1.12\lambda Lf/V. \tag{1}$$

Here, Θ_p is the AO diffraction angle; λ is the light wavelength; L is the AO interaction length; and f and V are, respectively, the frequency and speed of sound. It follows from (1) that, in order to increase $\Delta\Theta_p$ and decrease d_{min} at specified V and L values, one must reduce the sound frequency f. When diffraction efficiency is high, the angular range $\Delta\Theta_p$ slightly narrows, but even in this case the sound frequency must be reduced in order to increase $\Delta\Theta_p$ and decrease d_{min} [5, 6].

A TeO_2 AO cell was used to select a two-dimensional image edge in [1, 2]; this cell made it possible to implement AO interaction in tangential geometry. For the light with a wavelength $\lambda = 0.63$ μm, diffraction occurred at a frequency of 97.9 MHz. A collinear geometry of AO diffraction in a $CaMoO_4$ crystal was investigated in [3, 4]. Here, the sound frequency for the same light wavelength was lower: 46.6 MHz. Second- and third-order Bragg diffractions in TeO_2 were applied to select a two-dimensional edge in [7, 8]. For $\lambda = 0.63$ μm, the sound frequencies were 35 and 27 MHz, respectively. A more complex diffraction version, based on summation of two diffracted waves in crystal, was used in [9]. In that version, optical modes diffract at the same side with respect to the incident light beam. The sound frequency was ~27 MHz. At lower frequencies, light energy started being transferred to higher orders. In this case, the theoretical calculation is significantly complicated and, instead of quartic algebraic equations, one must solve sextic and higher order equations.

In this paper, we describe another diffraction version, which is implemented in TeO_2 at a sound frequency of ~9.5 MHz for light with $\lambda = 0.63$ μm; in this case, light energy transfer to higher orders is absent. The version is based on application of the so-called polarisation-independent Bragg diffraction [10–13], where intrinsic optical waves, undergoing anisotropic diffraction, deviate at different sides from the incident light beam. This regime is implemented at the angles of incidence of light corresponding to the regime of minimum anisotropic diffraction in TeO_2 [6], which is characterised by high angular selectivity and, therefore, excludes diffraction into higher orders. To date, the aforementioned frequency is minimal among all the frequencies used to select a two-dimensional image edge. In other words, the proposed version, in which an AO element is used as a Bragg filter of spatial frequencies, provides the maximum possible $\Delta\Theta_p$ value and the minimum d_{min} value.

2. Calculation

The vector diagram for the diffraction version in use is shown in Fig. 1. Here, radiation with a wave vector $\boldsymbol{K}$ is incident on the crystal optical face XY at an angle α. After entering the crystal, the radiation is split into two eigenwaves with wave vectors $\boldsymbol{K}_1$ and $\boldsymbol{K}_2$. Anisotropic diffraction of light waves occurs on the same sound wave with a wave vector $\boldsymbol{q}$. Waves $\boldsymbol{K}_1$ and $\boldsymbol{K}_2$ are diffracted in the direction of waves $\boldsymbol{K}_3$ and $\boldsymbol{K}_4$, respectively. The diffraction events occur with Bragg mismatch. The mismatch vectors are denoted as $\Delta\boldsymbol{k}_1$ and $\Delta\boldsymbol{k}_2$. Note that the version under consideration differs from the versions of polarisation-independent diffraction [10–13], in which waves $\boldsymbol{K}_1$ and $\boldsymbol{K}_2$ propagate collinearly. In our case, the waves are refracted at the crystal boundary Y at different angles, and the components of waves $\boldsymbol{K}$, $\boldsymbol{K}_1$, and $\boldsymbol{K}_2$ in the Y plane are equal, in correspondence with the refraction law [14]. Under these conditions, the theoretical calculation is significantly simplified [15].

V.M. Kotov, S.V. Averin, E.V. Kotov V.A. Kotel'nikov Institute of Radio Engineering and Electronics (Fryazino Branch), Russian Academy of Sciences, pl. Vvedenskogo 1, 141190 Fryazino, Moscow region, Russia; e-mail: vmk277@ire216.msk.su

Received 8 December 2017; revision received 9 January 2018
Kvantovaya Elektronika **48** (6) 573–576 (2018)
Translated by Yu.P. Sin'kov

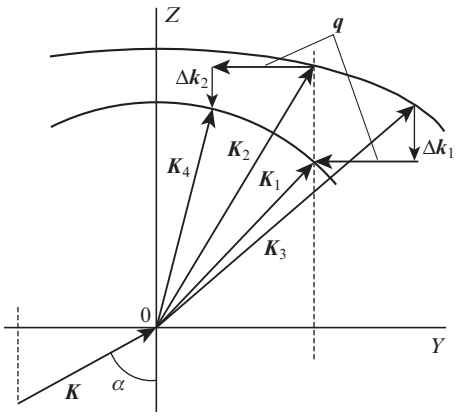

Figure 1. Vector diagram of polarisation-independent Bragg diffraction: Z is the crystal optical axis; XY is the crystal optical face; $\boldsymbol{K}, \boldsymbol{K}_1$ and $\boldsymbol{K}_2$ are the wave vectors of light beams incident on the crystal and refracted in it, respectively; α is the angle of incidence of beam $\boldsymbol{K}$ on the XY face (components $\boldsymbol{K}, \boldsymbol{K}_1$ and $\boldsymbol{K}_2$ in the XY face are mutually equal); $\boldsymbol{K}_3$ and $\boldsymbol{K}_4$ are the diffracted beams; $\Delta\boldsymbol{k}_1$ and $\Delta\boldsymbol{k}_2$ are the Bragg mismatch vectors; and $\boldsymbol{q}$ is the sound wave vector.

We assume that the transfer function is formed as a result of adding the amplitudes of waves $\boldsymbol{K}_1$ and $\boldsymbol{K}_2$, which can be considered as zero orders of Bragg diffraction. These amplitudes are given by the expressions [6, 15]

$$C_{1,2} = \left[\cos\left(\sqrt{\Delta k_{1,2}^2 + A_{1,2}^2}\,\frac{L}{2}\right) + \mathrm{i}\frac{\Delta k_{1,2}}{\sqrt{\Delta k_{1,2}^2 + A_{1,2}^2}} \times \sin\left(\sqrt{\Delta k_{1,2}^2 + A_{1,2}^2}\,\frac{L}{2}\right)\right]\exp\left(-\mathrm{i}\frac{\Delta k_{1,2}}{2}L\right), \quad (2)$$

where $\Delta k_{1,2}$ are Bragg mismatches; $A_{1,2} = v(Lf_{1,2})^{-1}$ are coupling coefficients;

$$v \approx \frac{2\pi}{\lambda}\sqrt{\frac{M_2 L}{2H}P_{\mathrm{ac}}} \quad (3)$$

is the Raman–Nath parameter [6]; H is the acoustic column height; M_2 is the coefficient of AO quality of material; P_{ac} is the acoustic power;

$$f_1 = \frac{1+\rho_1\rho_3}{\sqrt{1+\rho_1^2}\,\sqrt{1+\rho_3^2}}, f_2 = \frac{1+\rho_2\rho_4}{\sqrt{1+\rho_2^2}\,\sqrt{1+\rho_4^2}} \quad (4)$$

are the coefficients taking into account the ellipticity of optical waves [15]; and ρ_1, ρ_2, ρ_3, and ρ_4 are the ellipticities of waves K_1, K_2, K_3, and K_4, respectively. The ellipticities were calculated from the relation [15]

$$\rho = \frac{1}{2G_{33}}\left[\sqrt{\tan^4\theta(n_{\mathrm{o}}^{-2} - n_{\mathrm{e}}^{-2})^2 + 4G_{33}^2} - \tan^2\theta(n_{\mathrm{o}}^{-2} - n_{\mathrm{e}}^{-2})\right], \quad (5)$$

Here, G_{33} is a component of the gyration pseudotensor, n_{o} and n_{e} are the principal refractive indices of the crystal, and θ is the angle between the wave vector of light and the optical axis of the crystal. Since waves $\boldsymbol{K}_1$, $\boldsymbol{K}_2$, $\boldsymbol{K}_3$ and $\boldsymbol{K}_4$ propagate at different angles θ, their ellipticities generally differ. To determine the mismatches Δk_1 and Δk_2, which enter expression (2), we used the model of the indicatrix of a uniaxial gyrotropic crystal, expressed in terms of the components of the wave vector of light along the X, Y, and Z axes [15]:

$$k_z^4\left[\frac{1}{k_{\mathrm{o}}^4} - \left(\frac{\lambda}{2\pi}\right)^4 G_{33}^2\right] + T^2 N\left(\frac{k_z^2}{k_{\mathrm{o}}^2} - 1\right) + \frac{T^4}{k_{\mathrm{o}}^2 k_{\mathrm{e}}^2} - \frac{2k_z^2}{k_{\mathrm{o}}^2} + 1 = 0. \quad (6)$$

Here, $T = \sqrt{k_x^2 + k_y^2}$; k_x, k_y, and k_z are, respectively, the components of the wave vector of light $\boldsymbol{K}_j$ ($j = 1-4$) along the X, Y, and Z axes; $k_{\mathrm{o}} = 2\pi n_{\mathrm{o}}\lambda^{-1}$; $k_{\mathrm{e}} = 2\pi n_{\mathrm{e}}\lambda^{-1}$; and $N = k_{\mathrm{o}}^{-2} + k_{\mathrm{e}}^{-2}$.

For specific calculations, we assumed that the light wavelength is 0.63 μm and that light propagates in a TeO_2 crystal with the following parameters $n_{\mathrm{o}} = 2.26$, $n_{\mathrm{e}} = 2.41$, and $G_{33} = 2.62 \times 10^{-5}$. Diffraction occurs on a 'slow' sound wave propagating with a speed $V = 617$ m s^{-1}. With these parameters, $M_2 = 1200 \times 10^{-18}$ s^3 g^{-1} [16]. The sound field characteristics are as follows: $L = 0.6$ cm, $H = 0.4$ cm, and $P_{\mathrm{ac}} = 36$ mW. The sound frequency is 9.5 MHz. Under these conditions, the spatial-frequency bandwidth calculated from expressions (1) is $\Delta f_{\mathrm{p}} = 160$ cm^{-1}, which is an order of magnitude larger than that obtained in [1, 2].

Note that, according to our calculations, strict phase matching of two eigenwaves is obtained at a sound frequency of 9.48 MHz and an angle of incidence of light on the crystal $\alpha = 6.12°$ [15]. To form a transfer function, we used a somewhat higher frequency (it was taken to be 9.5 MHz). Due to this, we could 'expand' the transfer function after summing two optical fields along the sound wave propagation direction.

Figure 2 shows the transfer function for the zero Bragg order, calculated using the aforementioned parameters. The field angular size in Fig. 2 is $4° \times 4°$. The field is a set of circles having a common centre, onto which a dark oval area is imposed; the latter is due to strong attenuation of beams $\boldsymbol{K}_1$ and $\boldsymbol{K}_2$ as a result of their diffraction from the acoustic wave. This area is shifted relative to the centre of circles. It has an almost circular symmetry, which allows one to obtain a two-dimensional image edge without any significant distortions. Note also that the character of the field distribution depends on the total crystal length, because the light beam crosses the entire crystal rather than only the AO interaction region. The crystal length was taken to be 1 cm in the calculations. In addition, it was assumed that a polariser oriented at an angle β with respect to the Y axis is installed at the crystal output in

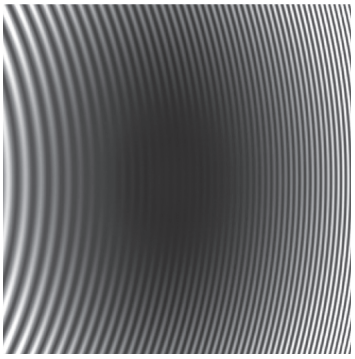

Figure 2. Transfer function of the zero diffraction order.

the XY plane. The field distribution presented in Fig. 2 was obtained at $\beta = 10°$.

Figure 3 shows examples of fast Fourier transform (FFT) processing of images in the form of rectangle, circle, and §§§ symbol. The distribution shown in Fig. 2 was used as a filter in this case. It can be seen that the lower patterns are clearly shaped two-dimensional contours.

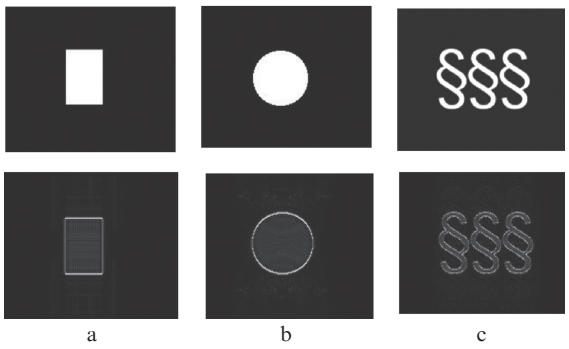

Figure 3. FFT processing of images in the form of (a) rectangle, (b) circle, and (c) §§§ symbol, using the transfer function shown in Fig. 2. The top and bottom patterns are, respectively, images before and after FFT processing.

3. Discussion of experimental results

Figure 4 shows a schematic of the experimental setup that was used to implement optical Fourier image processing. A wide light beam I_0, propagating in a direction close to the Z axis, arrives at screen A1; a hole in this screen serves as the initial image. The light transmitted through the hole is directed to lens L1 with a focal length F. An AO cell located behind the lens plays the role of a spatial-frequency filter. An acoustic wave propagates in the cell along the Y direction. The cell operates in the regime providing polarisation-independent AO diffraction. The optical rays emerging from the AO cell, which are lie in the diffraction plane YZ, are directed to lens L2 (identical to lens L1). Images obtained by Fourier processing are observed on output screen A2. Polariser P is installed between lens L2 and output screen A2. The distances between elements A1, L1, AO, L2, and A2 are equal to the focal length F of the lenses. Lens L1 performs a Fourier transform, and lens L2 carries out a repeated Fourier transform, which is equivalent to the inverse Fourier transform with coordinate inversion. In the general case, images formed in the zero, +1st, and –1st diffraction orders are observed on screen A2. Varying the sound frequency f, as well as the sound power and angular orientation of the AO cell, one can change the intensity distribution in all images.

The light source was a He–Ne laser, generating linearly polarised 0.63-μm radiation. The initial image was that of an almost round hole ~1 mm in diameter, made by a needle in aluminium foil. The foil with hole was located in the A1 plane. The lens focal length was $F = 16$ cm. The result of the Fourier processing was observed on screen A2, located in the focal plane of output lens L2. A paratellurite AO cell, operating in the regime of polarisation-independent diffraction, served as a spatial-frequency filter. The crystal sizes were $1.0 \times 1.0 \times 1.0$ cm along the [110], [1$\bar{1}$0], and [001] directions, respectively, which correspond to the X, Y, and Z directions in Figs 1 and 4. The sound frequency f in the AO cell was 9.2 MHz, the speed of sound V was 0.617 m/s, and the electric voltage across the piezoelectric transducer was 4.4 V. The best conditions for selecting an image edge were implemented when polariser P was oriented at an angle $\beta = 45°$.

Figure 5 shows the images observed on the screen in the absence and in the presence of sound. The bright spots in Fig. 5b correspond to three diffraction orders: zero, +1st, and –1st. One can clearly see an image edge in the zero diffraction order. Its quality is sufficiently high in both vertical and horizontal directions. Thus, in our opinion, the experiments clearly confirm the efficiency of polarisation-independent diffraction for two-dimensional filtering of optical images. The photograph in Fig. 5b demonstrates also that the efficiencies of the +1st and –1st diffraction orders differ. This difference is explained by the rather strong asymmetry of the dependence of mismatch on the angle of incidence of light on the crystal for the diffractions into the 1st and –1st orders. Other discrepancies between the theory and experiment results can be explained by errors of the model in use, crystal inhomogeneity, etc. In any case, the experimental data are in good agreement with theoretical predictions.

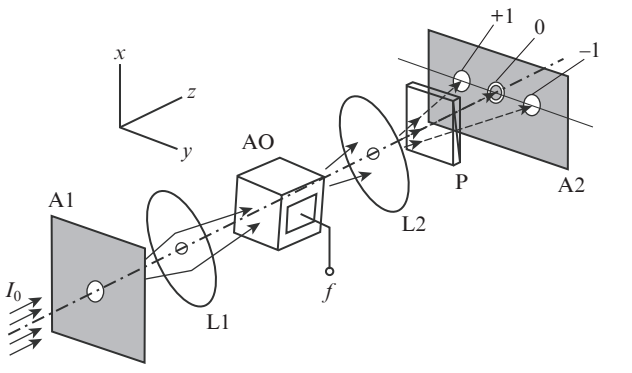

Figure 4. Optical scheme of the experiment: (A1, A2) planes of input and output images, (L1, L2) lenses, (AO) acousto-optic cell, and (P) polariser; the +1st, zero, and –1st diffraction orders in the A2 plane are shown.

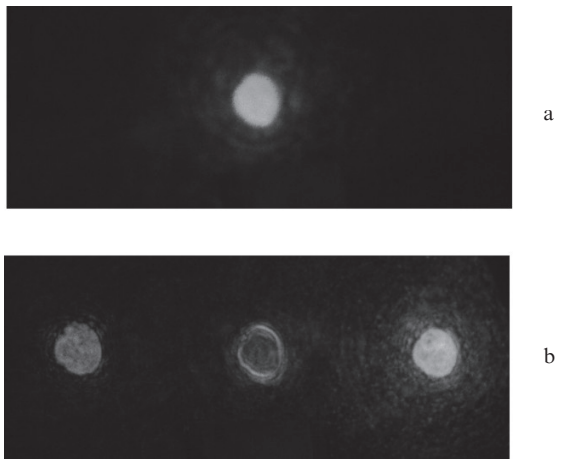

Figure 5. Result of Fourier processing of the image: the output image observed on screen A2 (a) in the absence and (b) in the presence of a sound wave. The middle image is zero Bragg order; the images on the right and left correspond to the +1st and –1st orders, respectively.

4. Conclusions

Based on the aforesaid, we can draw the following conclusions.

1. To select a two-dimensional edge of an optical image, it was proposed to use the regime of polarisation-independent diffraction, where crystal eigenwaves diffract into the +1st and –1st orders as a result of anisotropic AO interaction. This regime is implemented in uniaxial gyrotropic crystals at angles of incidence of light close to those at minimum Bragg diffraction, which is characterised by high angular selectivity and, therefore, excludes diffraction into higher orders. When using a TeO_2 single crystal to process an image with a wavelength of 0.63 μm, the sound frequency turned out to be ~9.5 MHz. To date, this is the minimum frequency at which the maximum possible transmission bandwidth of spatial frequencies and minimum resolved size of AO element can be obtained.

2. The fragment of the transfer function of the zero diffraction order providing selection of a two-dimensional edge when optical image processing was theoretically calculated. The efficiency of this fragment as a spatial-frequency filter in FFT image processing was demonstrated.

3. The selection of an edge in the zero diffraction order using Fourier processing of an optical image with a wavelength of 0.63 μm was experimentally demonstrated. Here, an AO cell made of TeO_2 single crystal, operating at a sound frequency of ~9.2 MHz, served as a spatial-frequency filter.

Acknowledgements. This work was supported in part by the Russian Foundation for Basic Research (Grant No. 16-07-00064).

References

1. Balakshy V.I., Voloshinov V.B. *Quantum Electron.*, **35**, 85 (2005) [*Kvantovaya Elektron.*, **35**, 85 (2005)].
2. Balakshy V.I., Voloshinov V.B., Babkina T.M., Kostyuk D.E. *J. Mod. Opt.*, **52**, 1 (2005).
3. Balakshy V.I., Mantsevich S.N. *Opt. Spektrosk.*, **103**, 831 (2007).
4. Balakshy V.I., Kostyuk D.E. *Appl. Opt.*, **48**, C24 (2009).
5. Balakshy V.I. *Radiotekh. Elektron.*, **29**, 1610 (1984).
6. Balakshy V.I., Parygin V.N., Chirkov L.E. *Fizicheskie osnovy akustooptiki* (Physical Principles of Acousto-Optics) (Moscow: Radio i Svyaz', 1985).
7. Kotov V.M., Shkerdin G.N., Bulyuk A.N. *Quantum Electron.*, **41**, 1109 (2011) [*Kvantovaya Elektron.*, **41**. 1109 (2011)].
8. Kotov V.M., Shkerdin G.N., Averin S.V. *Radiotekh. Elektron.*, **61**, 1090 (2016).
9. Kotov V.M., Averin S.V., Kuznetsov P.I., Kotov E.V. *Quantum Electron.*, **47**, 665 (2017) [*Kvantovaya Elektron.*, **47**, 665 (2017)].
10. Lee H. *Appl. Opt.*, **27**, 815 (1988).
11. Voloshinov V.B., Molchanov V.Ya. *Opt. Laser Technol.*, **27**, 307 (1995).
12. Voloshinov V.B., Molchanov V.Ya., Mosquera J.C. *Opt. Laser Technol.*, **28**, 119 (1996).
13. Molchanov V.Ya., Kitaev Yu.I., Kolesnikov A.I., Narver V.N., Rozenshtein A.Z., Solodovnikov N.P., Shapovalenko K.G. *Teoriya i praktika sovremennoi akustooptiki* (Theory and Practice of Modern Acousto-Optics) (Moscow: MISiS, 2015).
14. Born M., Wolf E. *Principles of Optics: Electromagnetic Theory of Propagation, Interference, and Diffraction of Light* (Oxford: Pergamon, 1964; Moscow: Nauka, 1973).
15. Kotov V.M. *Akustooptika. Breggovskaya difraktsiya mnogotsvetnogo izlucheniya* (Acousto-Optics. Bragg Diffraction of Multicolor Radiation) (Moscow:Yanus-K, 2016).
16. Shaskol'skaya M.P. (Ed.) *Akusticheskie kristally* (Acoustic Crystals) (Moscow: Nauka, 1982).